Supporting Information Corrected October 27, 2014

Figure Legends, Supplemental Computational/Experimental Procedures/Analysis

Utilization of extracellular information before ligand-receptor binding reaches equilibrium expands and shifts the input dynamic range.

Alejandra C Ventura, Alan Bush, Gustavo Vasen, Matías A Goldín, Brianne Burkinshaw, Nirveek Bhattacharjee, Albert Folch, Roger Brent, Ariel Chernomoretz, and Alejandro Colman-Lerner

Table of contents.

Supplemental Figures directly called from the main text. 3
Figure S1. Toy models with transient signaling modules perform PRESS, related to Figure 2. 3
Figure S2. The effect of noise during PRESS, related to Figure 2. 4
Figure S3. Characterization of PRESS applied to gradient detection, related to Figure 3. 5
Figure S4. Timing of yeast polarization, related to Figure 3. 6
Figure S5. Timing of polarization patch relocalization, related to Figure 3. 7
Figure S6. The αF receptor binding dynamics might be optimal for PRESS, related to Figure 4 8
1. Characterization of the ligand-receptor time-dependent dose-response curve. 9
2. Toy models with transient signaling modules perform PRESS 11
Model 1: X with an inactive refractory state. 11
Model 2: X controlled by an incoherent feed-forward loop (IFFL); and Model 3: X controlled by a negative feed-back loop (NFBL). 11
3. Models with transient signaling may be subsensitive, helping to expand the input dynamic range. 13
Sensitivity in Model 1: X with an inactive refractory state. 13
Table S1. Model 1 sensitivity. 14
Sensitivity in Model 3: X controlled by a negative feed-back loop (NFBL). 15
Table S2. Model 3 sensitivity. 15
General conclusions based on the above studies and the results in the main text: 15
4. The effect of noise during PRESS 18
5. Mathematical model to study the sensing of a stationary spatial gradient 20
5.1 An analytical expression for the αF gradient generated by a point source, and for the variable Delta (Description 1) 20
5.1.1 A simplified formula for the αF gradient generated by a point source, and the variable Delta 23
5.2 An analytical expression for the variable Delta (Description 2) 25
Table S3. Strains. 28
6 Supplemental experimental procedures 28
6.1 Strains and plasmids. 28
6.2 Quantification of Polarization Times 29
7. Triple monomeric NeonGreen DNA sequence 30
8. Supplemental References 31

Supplemental Figures directly called from the main text.

Figure S1. Toy models with transient signaling modules perform PRESS, related to Figure 2.

In the three models, left panels contain schemas of the corresponding model, middle panels show dose-responses and right panels show temporal dynamics. Parameters were selected so that X* has a transient behavior. Dose-responses are included for the equilibrium value of C (ligand-receptor complex) in solid black lines, and for the maximum of X* in dashed blue lines. The dose of the ligand is normalized by the K_d of the binding/unbinding reaction. Temporal profiles of C (solid lines) and of X* (dashed lines) are included at ligand concentrations indicated over the traces.

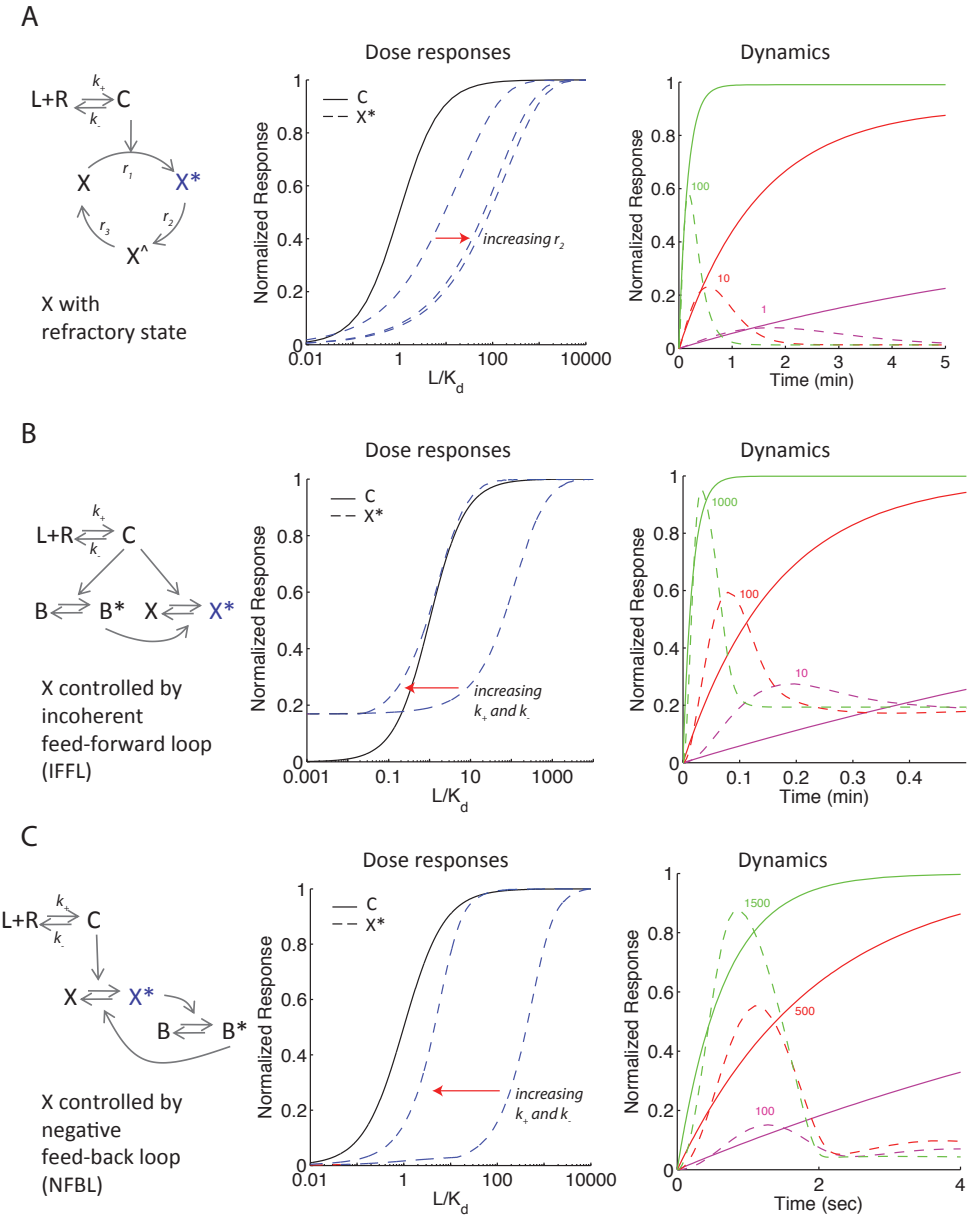

A. X with an inactive refractory state (same as in Figure 2). **Left.** Occupied receptor activates effector X; after a while, active X (X*) converts into an inactive refractory state (X^), which slowly converts back to the inactive form (X), closing the cycle. **Middle**. Parameter values: k_-=0.001 1/sec, r_1=0.1, r_2=0.06-0.8-1.6 (increasing from left to right in the middle panel), r_3=0.001, X_{tot}=10 (k_+ is not needed because of the dimensionless variables chosen, see section 1). EC50 for each response: 1 for C, and for X* is 9.3 for r_2=0.06, 65.8 for r_2=0.8, and 87 for r_2=1.6. **Right**. Temporal profiles for the same parameters as in the middle panel, using r_2=0.8.

B. X controlled by an incoherent feed-forward loop (IFFL). **Left.** Occupied receptor activates both B and X into B* and X*, and B* increases X* inactivation. **Middle**. Parameter values: k_-=0.001-0.1 1/sec (from right to left), k_{CB}=0.5, K_{CB}=0.01, k_{FBB}=10, K_{FBB}=10, F_B=0.5, k_{CX}=2, K_{CX}=0.1, k_{BX}=3, K_{BX}=0.1 (see SI Appendix, Section 2 for details of the model, k_i are catalytic rate constants and K_i are Michaelis-Menten constants, for example, k_{CB} and K_{CB} are the pair characterizing how C regulates B). **Right**. Temporal profiles for the same parameters as in the middle panel, using k_-=0.001 1/sec.

C. X controlled by a negative feed-back loop (NFBL). **Left.** Occupied receptor activates X into X*, X* activates B into B*, and B* increases X* inactivation. **Middle**. Parameter values: k_-=0.001-0.1 1/sec (from right to left), k_{XB}=1, K_{XB}=0.01, k_{FBB}=5, K_{FBB}=100, F_B=0.5, k_{CX}=5, K_{CX}=0.1, k_{BX}=6, K_{BX}=0.01 (see SI Appendix, Section 2 for details of the model). **Right**. Temporal profiles for the same parameters as in the middle panel, using k_-=0.001 1/sec.

Figure S2. The effect of noise during PRESS, related to Figure 2.

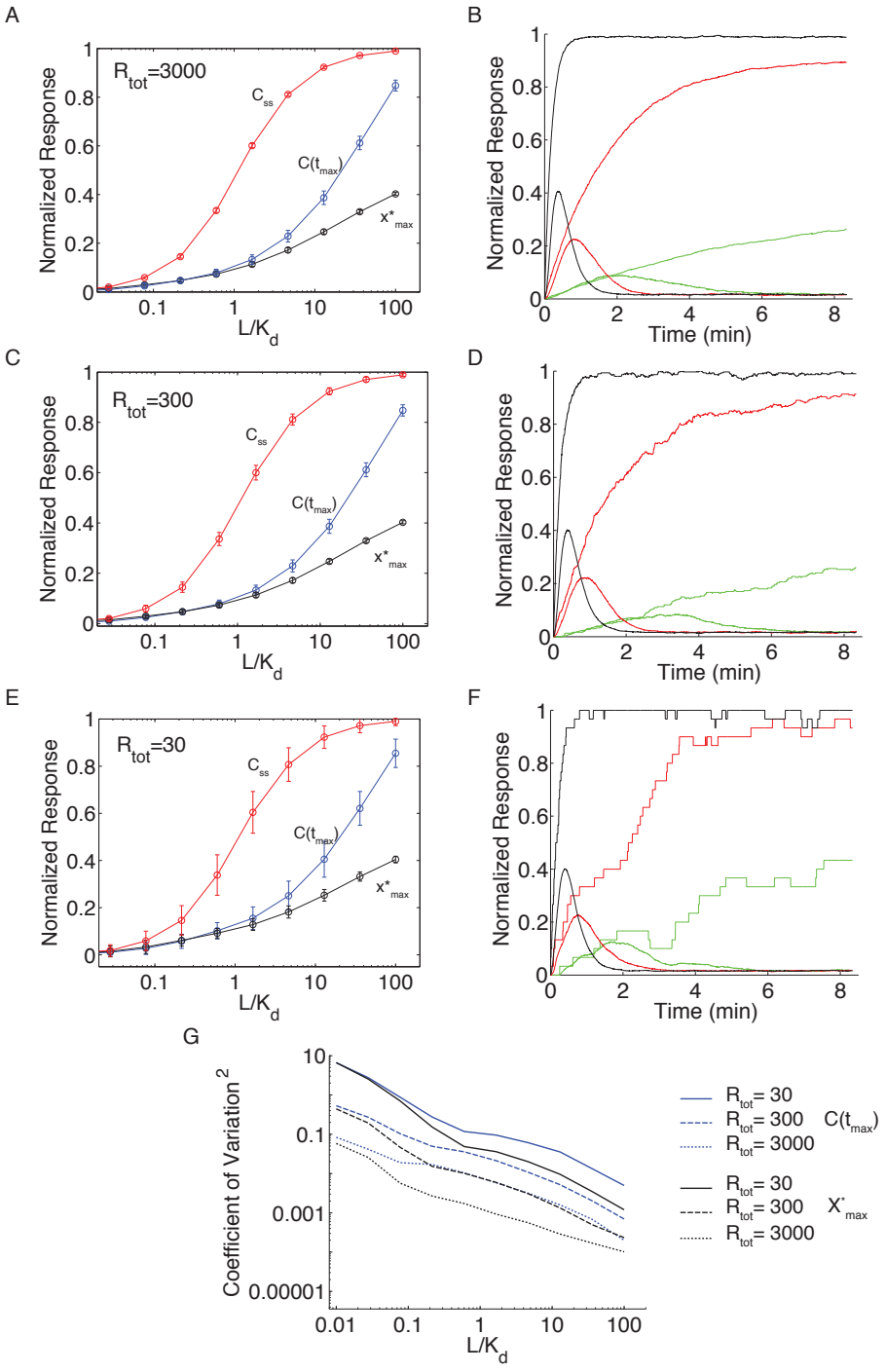

Results of simulating Model 1 (the model with an inactive refractory state) for low, medium, and high number of receptors (30-300-3000), using stochastic methods. Simulations were done in Copasi using its adaptive tau-leaping algorithm. Parameter values: k_+=0.0002 ml/(pmol*sec), k_-=0.001 1/s, r_1=0.01 ml/(pmol*sec), r_2=0.06 1/sec, r_3=0.001 1/sec (with 1 pmol/ml = 1 nM). Initial particle numbers: receptor=30-300-3000, x=14536.5. Cell volume= 5e-11 ml. Left panels (A, C and E) contain normalized dose-response curves and right panels (B, D and F) contain normalized temporal profiles, A and B correspond to 3000, C and D to 300 and E and F to 30 receptors per cell, as indicated over the figure. **Left panels**: Equilibrium value of the ligand-receptor complex C (C_{ss}) in red dashed lines, maximum of X* (X^*_{max}) in black dashed lines, and C at the time where X* reaches its maximum ($C(t_{max})$) in blue dashed lines. The dose of the ligand is normalized by the K_d of the binding/unbinding reaction. Open circles and error bars correspond to mean value and standard deviation over N=1001 stochastic simulations performed with the same set of parameter values for each value of ligand, 9 values of ligand were considered in the range 0.05-500 nM (corresponding to 0.01-100 L/K_d). **Right panels**: L/K_d=1-10-100 K_d are indicated in green, red, black, respectively. Monotonic curves correspond to the ligand-receptor complex C, curves with transient behavior correspond to X*. Both in left and right panels curves were normalized as follows: C_{eq} and $C(t_{max})$ were divided by the initial receptor particle number and X* was divided by the initial X particle number. **G**: CV^2 (coefficient of variation, the ratio of the standard deviation to the mean, squared) versus normalized ligand, for 3000-300-30 receptors per cell (dotted, dashed, solid lines, respectively). CV^2 for $C(t_{max})$ in blue, and for X^*_{max} in black.

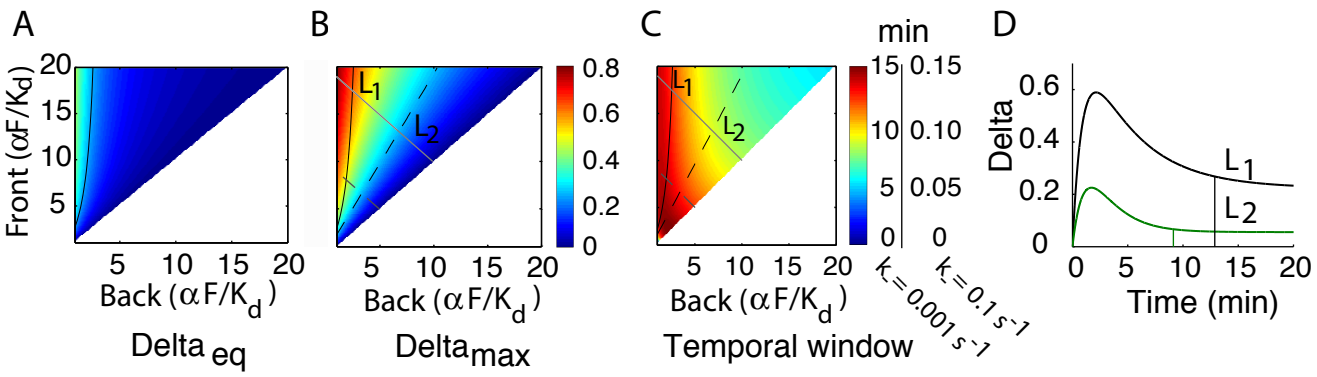

Figure S3. Characterization of PRESS applied to gradient detection, related to Figure 3.

A-C. Graphs are heatmaps of $Delta_{eq}$ (A), $Delta_{max}$ (B) and temporal window (C) as functions of $\widetilde{\alpha F}_f$ and $\widetilde{\alpha F}_b$ (αF_f and αF_b divided by the K_d). Since we are considering gradients, αF_f has to be greater than αF_b (and this is why the figure is blank below the diagonal). $Delta_{eq}$ and $Delta_{max}$ were calculated using the analytical calculation in the SI Appendix, and are plotted using the same color scale. The temporal window was numerically calculated as the interval during which Delta is more than 1.2 $Delta_{eq}$. We show two color scales, obtained with the indicated unbinding rates k_-. The black solid line over each panels corresponds to $Delta_{eq}$ = 0.23 and the black dashed line corresponds to $Delta_{max}$ = 0.23. The solid grey line represents a gradient with an average between front and back of 10 K_d and the dashed grey line, 5 K_d. A cell sensing with an average 10 K_d could have different combinations of $\widetilde{\alpha F}_b$ and $\widetilde{\alpha F}_f$, some of them will result in $Delta_{max}$ > 0.23 and $Delta_{eq}$ < 0.23 (those that correspond to the grey solid line in the region between the solid and dashed black lines). The intersections of the line representing an average of 10 K_d and the lines for $Delta_{eq}$ = 0.23 and $Delta_{max}$ = 0.23 are identified as **L_1** and **L_2**, respectively. **L_1** is characterized by $\widetilde{\alpha F}_f = 17.4$ and $\widetilde{\alpha F}_b = 2.6$, resulting in $Delta_{eq}$=0.23 and $Delta_{max}$=0.59, respectively, and a temporal window of 12.9 min. **L_2** is characterized by by $\widetilde{\alpha F}_f = 13.1$ and $\widetilde{\alpha F}_b = 6.9$, respectively, resulting in $Delta_{eq}$ = 0.06 and $Delta_{max}$ = 0.23 and a temporal window of 9.1 min. **D.** Delta(t) vs time, for **L_1** and **L_2**. The vertical line indicates the time were the temporal window for PRESS ends.

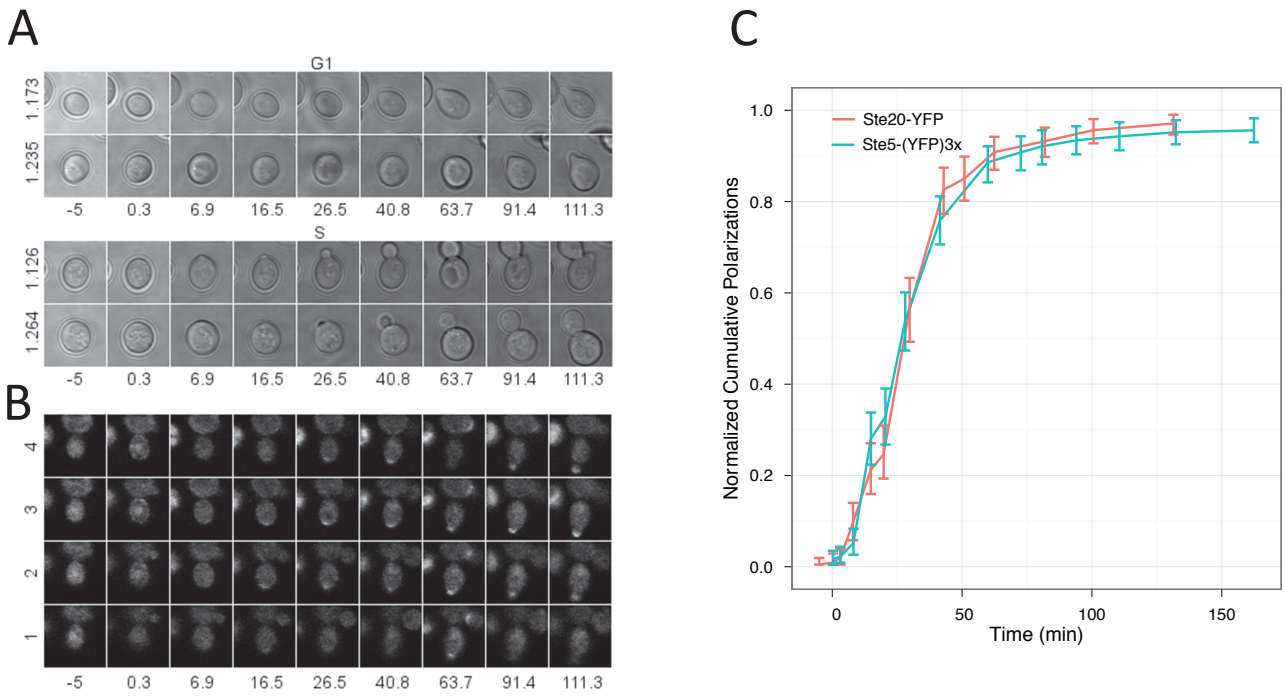

Figure S4. Timing of yeast polarization, related to Figure 3.

A. Example of a transmission image montage used to determine the position in the cell cycle (YPP3662 strain, 1µM α-factor). G1 cells (top) respond to pheromone forming a mating projection. S cells (bottom) first bud and then respond to pheromone. Time in minutes is shown below each image, and the ID of each cell is shown on the left.

B. Example of a YFP image montage used to determine the polarization time (YPP3662 strain, 1µM α-factor). The slice number of the Z stack is indicated on the left. Time in minutes is shown below each image.

C. Cumulative fraction of polarized cells vs. time for Ste5-YFPx3 (YPP3662) or Ste20-YFP (ESY3136). Cells were stimulated with 1µM α-factor at time zero. Only cells in G1 were considered for this analysis. Error bars represent the 95% confidence interval of the mean as calculated by bootstrap.

Figure S5. Timing of polarization patch relocalization, related to Figure 3.

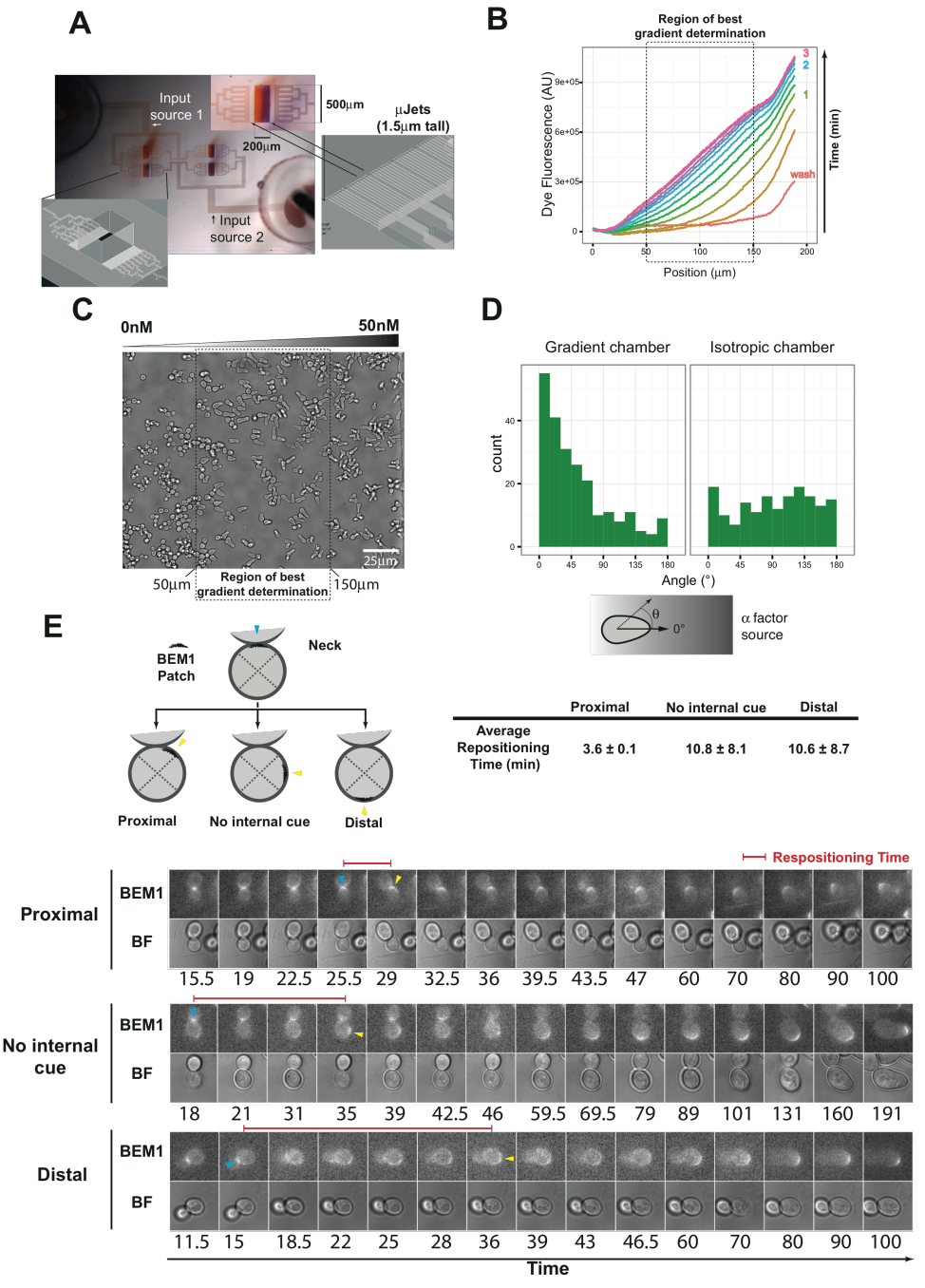

	Proximal	No internal cue	Distal
Average Repositioning Time (min)	3.6 ± 0.1	10.8 ± 8.1	10.6 ± 8.7

A. The microfluidic device we used. It contains two ports, one filled with a red dye (labeled input source 1) and the other one with a blue dye (labeled input source 2), and 4 open chambers (200 x 500 µm). Two of the chambers receive different inputs, and a gradient is formed; the other two serve as controls.The fluid is delivered to the wells by a binary splitting manifold that ends in a line of 38 microjets of 10 µm wide and 2.5 µm tall. **B.** The dynamics of gradient formation. We formed a gradient using a solution of BPB (bromophenol blue, 0.01%) as source 1 and water as source 2. We determined the gradient profile measuring BPB fluorescence using a standard Texas Red filter cube. At t=0, we washed away the chamber with a pipet and then we monitored gradient formation by imaging every 15 seconds. The gradient is linear and it reaches the steady state in ~3 min.

C. Brightfield image of yeast strain ACL379 exposed to a gradient of 0-50nM of αF for 3 hours. The middle region of the chamber displays the highest percentage of cells oriented in the direction of the gradient.

D. Histogram showing the quantification of the angles between the shmoo and the direction of the gradient. Perfectly aligned cells display an angle of 0°. The isotropic chamber (right) has no bias in the angle, as expected for random polarization (uniform external cue).

E. Diagram representing the measurement of patch repositioning time. Newly divided cells show Bem1 polarization at the bud-neck. In response to α factor exposure, Bem1 forms a new patch somewhere in the cell periphery. Depending on the position of the new polarization, patches (both in mothers or daughters) were classified as "proximal", "distal" or "no internal cue". The time (in minutes) between the last frame with bud-neck polarization and the first with a new visible patch was used to estimate the repositioning time. We show an example of each group of yeast YGV5097 (expressing Bem1-mNG$_{(3x)}$) (blue arrowheads indicate the polarization in the neck, yellow arrowheads show a new patch and the repositioning time is delineated by the red line). Average repositioning time is presented in the table (mean ± standard deviation).

Figure S6. The αF receptor binding dynamics might be optimal for PRESS, related to Figure 4.

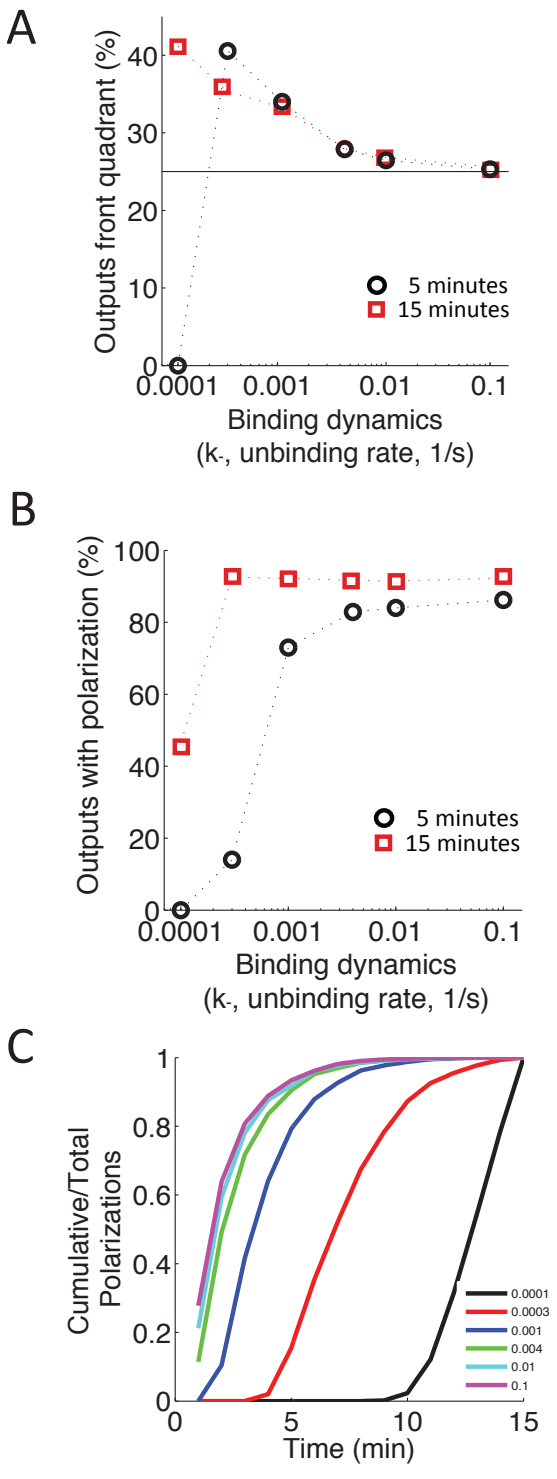

A. Percentage of polarizations in the front quadrant as a function of binding dynamics (parameter *k-*), using $\frac{q/4\pi Dd}{K_d} = 10$ and $\frac{a}{d} = 0.3$ (corresponding to p_1=10 and p_2=0.3, see SI Appendix, Section 5), as in Fig. 4D. For each value of k_-, we run a set of stochastic numerical simulations (Altschuler's model with external gradient as input), and counted the number of runs that resulted in a polarized state, and then determined how many polarized in the quadrant facing the αF source (front quadrant). We computed polarizations that took place in the first five minutes of the simulation as in Fig 4D (black circles) or in the total simulation time of fifteen minutes (red circles). We varied parameter k_- from 0.0001 1/sec to 0.1 1/sec (this last value corresponding to the "fast" receptor in Fig. 4D). A horizontal line over the plot indicates the expected percentage output if polarizations were randomly located, *i.e.* 25%. For fast receptor dynamics, the system is unable to use the gradient information. A receptor slower than wt results in improved sensing, but only allowing more time to polarize. When evaluating the polarization performance in 5 min (black circles) we found a maximum in the percentage outputs in the front quadrant at k_- of about 0.0003 1/sec. For the time window of 15 min instead, the maximum is achieved at the slower dynamics considered for this figure (k_-=0.0001 1/sec).

B. Percentage of polarizing cells as a function of parameter $\frac{q/4\pi Dd}{K_d} = 10$ and $\frac{a}{d} = 0.3$ (corresponding to p_1=10 and p_2=0.3, see SI Appendix, Section 5). As explained in (**A**), if the receptor dynamics is very slow, very few cells polarize in 5 min.

Combining the information in (**A**) and (**B**), we conclude that there is a tradeoff between achieving a good number of polarizing cells in a population and obtaining a good performance for those polarizations (in the sense that those cells correctly identify the position of the partner). If the decision has to be made in the first 5 minutes, then the dynamics corresponding to the a-factor receptor (k_-=0.001 1/sec) results in the best combination of polarizing cells with successful polarizations. For a longer time interval, like the one of 15 minutes analyzed, the optimal occurs for a still slower dynamics, k_- about 0.0003 1/sec.

C. Summation of all the polarizations that appeared for a time less or equal than the time indicated in the horizontal axis, normalized by the total number of polarizations achieved at the end of the simulation (t=15 min). Each value of k_- is indicated with a different color as shown in the figure.

The number of stochastic numerical simulations performed for each value of k_- is: 19,000 for k_-=0.0001 1/sec, 10280 for k_-=0.0003 1/sec, and 2000 for all the other values of k_-. Comparing the outputs for each two successive values of k_- indicate that only the following pairs are significantly different ($p < 0.05$): 0.0003-0.001, and 0.001-0.004 at 5 min; 0.0001-0.0003, and 0.001-0.004 at 15 min.

1. Characterization of the ligand-receptor time-dependent dose-response curve.

In this section we characterize the sensitivity and potency (given by parameters n_H and EC_{50}, respectively) of the curve that describes the time evolution of occupied receptor at different doses of ligand for the simple case of one-step binding, assuming that free L is not significantly affected by the reaction:

$$C_{(t,L)} = C_{eq(L)} * \left(1 - e^{(-t/\tau_{(L)})}\right)$$

with

$$C_{eq} = R_{tot}\frac{L}{L+K_d} = R_{tot}\frac{L/K_d}{L/K_d+1}$$

the steady-state value for C and

$$\tau = \frac{1}{k_- + L*k_+} = \frac{1}{k_-(1+\frac{L}{K_d})}$$

the characteristic time τ (time required to reach 63.2% of the steady-state value). L is the ligand, R is the receptor, C is the complex ligand-receptor, and k_+ and k_- are the binding and unbinding rates, respectively. Normalizing the curve C(t,L) by R_{tot} and defining $x=L/K_d$ (normalized ligand concentration), results in a function that depends only on x and k_-:

$$C_{(t,x)} = \frac{x}{1+x} * \left(1 - e^{(-t*k_-*(1+x))}\right)$$

The steady-state of this last function, which we obtained by taking the limit t->∞, has an n_H = 1 and EC_{50} = 1. We are interested in obtaining the EC_{50} and n_H for normalized C versus x, for any given time, which will result in two relationships: $EC_{50}(t)$ and $n_H(t)$. Instead of $EC_{50}(t)$ we could easily obtain the inverse function, $t(EC_{50})$, as follows:

$$t = \frac{1}{k_- * (1 + EC_{50})} \log\left(\frac{2 * EC_{50}}{EC_{50} - 1}\right)$$

Based on this last expression, we plot EC_{50} versus time in Fig. S7. According to this plot,

1. EC_{50} > 1 for every time, and EC_{50} = 1 only for the equilibrium binding curve;
2. EC_{50} decreases when time increases;
3. If k_- is large (fast unbinding reaction), the time at which the curve C versus x has a given EC_{50} is small. For example, if the desired EC_{50} is $10*K_d$, then, the dose response curve has that EC_{50} at around ~1 min for k_-=0.001 sec^{-1} and at ~0.1 min for k_-=0.01 sec^{-1}, see Fig. S7.

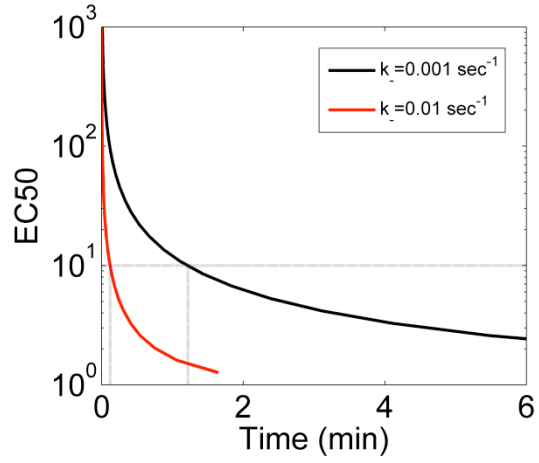

Figure S7. EC50 of L-receptor binding curve vs. Time. EC_{50} is in units of L/K_d.

Regarding the sensitivity of the normalized C versus x curve for times prior to reaching the equilibrium, we obtained an approximated n_H=1.4 in the limit of low values of $t*k_-$. We

obtained this value by deriving t(EC_{90}) and t(EC_{10}) in the same way we derived t(EC_{50}), and neglecting terms as follows:

$$t = \frac{-1}{k_- * (1 + EC_{10})} \log\left(\frac{EC_{10} * 0.9 - 0.1}{EC_{10}}\right) \sim \frac{-1}{k_- * (1 + EC_{10})} \log(0.9)$$
$$t = \frac{-1}{k_- * (1 + EC_{90})} \log\left(\frac{EC_{90} * 0.1 - 0.9}{EC_{90}}\right) \sim \frac{-1}{k_- * (1 + EC_{90})} \log(0.1)$$

These approximations are valid because at short times ($t*k_-<<1$), both EC_{90} and EC_{10} are much greater than one, similar to the behavior of EC_{50} (Figure S7). From the last two formulas we obtained the ratio EC90/EC10:

$$\frac{EC_{90}}{EC_{10}} = \frac{-\log(0.1) - t*k_-}{-\log(0.9) - t*k_-}$$

which results in 21.85 when $t*k_-$ is neglected, leading to n_H=1.42 (n_H=log(81)/log(EC_{90}/EC_{10}). This approximated result indicates that the sensitivity goes from about 1.4, in the limit of low values of $t*k_-$, to 1, in the limit of t->∞, and means that before reaching equilibrium the sensitivity is higher than when it is reached.

2. Toy models with transient signaling modules perform PRESS

Model 1: X with an inactive refractory state.

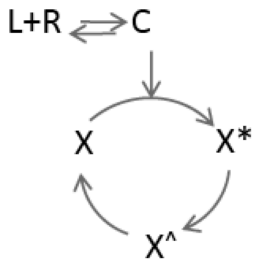

Figure S8. Toy model with a refractory state.
Toy model of a downstream response activated by the ligand-receptor complex. Occupied receptor activates effector X; after a while, active X (X*) converts into an inactive refractory state (X^), which slowly converts back to the inactive form (X), closing the cycle.

Occupied receptor activates effector X with a rate r_1; active X (X*) converts into an inactive refractory state (X^) with rate r_2, which converts back to the inactive form (X) with rate r_3, closing the cycle (see Fig. S8). Assuming that the total amount of X, X_{tot} = X + X* + X^ is conserved, the system is described by the following ordinary differential equations:

$$\frac{dX}{dt} = -r_1 XC + r_3(X_{tot} - X^* - X) \qquad (1)$$

$$\frac{dX^*}{dt} = r_1 XC - r_2 X^* \qquad (2)$$

where C is the ligand-receptor complex. The parameters used in the numerical simulations reported in Figs. 2a-b in the main text are r_1 = 0.1, r_2 = 0.8, r_3 = 0.001, X_{tot} = 10, and the initial condition was such that all the effector was initially in its inactive state X. The steady-state reached by this systems is characterized by $X^*_{eq}/X_{tot} = r_3/(r_3 + r_2 + r_2 r_3/(r_1 C_{eq}))$ and $X_{eq}/X_{tot} = r_2 r_3/(r_2 r_3 + r_1 C_{eq}(r_2 + r_3))$.

Model 2: X controlled by an incoherent feed-forward loop (IFFL); and Model 3: X controlled by a negative feed-back loop (NFBL).

The equations for the network depicted in Fig. S9 and Fig. S10 were adapted from those in Ma et al (1) for the case where one node is a ligand-receptor complex. We assume that each node (C, B, X) has a fixed concentration (normalized to 1) but has two forms: C is the ligand-receptor complex and (1-C) is the free receptor; B* and X* represent the concentration of active states, (1-B*) and (1-X*) are the concentration of the inactive states. L is the concentration of free ligand and k_+ and k_- are the binding and unbinding rates, respectively. k_{CB} and k_{CX} are the strength with which C activates B and X into B* and X*, and k_{BX} is the strength of the negative regulation from B* to X*. If a node has only positive incoming links, like node B in Fig. S9 and in Fig. S10, it is assumed that there is a background (constitutive) deactivating enzyme F_i of a constant concentration to catalyze the reverse reaction (see Ma et al (1) for details). The resulting equations

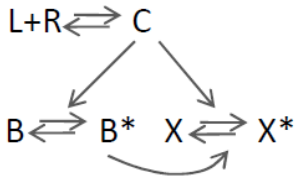

Figure S9. Toy model of an incoherent feedforward loop.
Occupied receptor activates both B and X, into B* and X*, respectively. B* regulates the inactivation of X* into X.

describing the network in Fig. S9 are:

$$\frac{dC}{dt} = k_+ \cdot L(1-C) - k\_\, C$$

$$\frac{dB^*}{dt} = k_{CB} \cdot C \frac{(1-B^*)}{(1-B^*)+K_{CB}} - k_{FBB} \cdot F_B \frac{B^*}{B^*+K_{FBB}}$$

$$\frac{dX^*}{dt} = k_{CX} \cdot C^* \frac{(1-X^*)}{(1-X^*)+K_{CX}} - k_{BX} \cdot B^* \frac{X^*}{X^*+K_{BX}}$$

The resulting equations describing the network in Fig. S10 are:

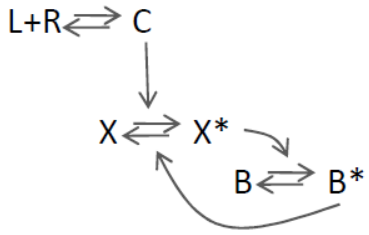

$$\frac{dC}{dt} = k_+ \cdot L(1-C) - k\_C$$

$$\frac{dB^*}{dt} = k_{XB} \cdot X^* \frac{(1-B^*)}{(1-B^*)+K_{XB}} - k_{FBB} \cdot F_B \frac{B^*}{B^*+K_{FBB}}$$

$$\frac{dX^*}{dt} = k_{CX} \cdot C \frac{(1-X^*)}{(1-X^*)+K_{CX}} - k_{BX} \cdot B^* \frac{X^*}{X^*+K_{BX}}$$

Figure S10. Toy model of a negative feedback loop.

Occupied receptor activates X into X*, X* activates B into B* and B* regulates the inactivation of X* into X.

3. Models with transient signaling may be subsensitive, helping to expand the input dynamic range.

Modulation of the input dynamic range could imply its **expansion/compression** (i.e., an increase or decrease of the range of doses where the system produces dose-dependent responses), its **displacement** (i.e., the ratio EC_{90}/EC_{10} is the same but it is centered around a different dose), or a combination of both. Expansion/compression of the dynamic range is determined by the sensitivity of the response, quantified by the change in the Hill coefficient n_H ($\log(81)/\log(EC_{90}/EC_{10})$) of the response: the higher the n_H, the smaller the input dynamic range. Displacement of the dynamic range is usually quantified by the change in the EC_{50} of the response. A rightward displacement of the EC_{50} with constant n_H enables dose-dependent responses in the high concentration range without compromising sensitivity, while a decrease in n_H with constant EC_{50} results in an extended range of dose-dependent responses and a corresponding loss of sensitivity, meaning that the difference in the output you get for two different stimuli is smaller than otherwise would have been.

The common Michaelis-Menten relationship gives, by definition, an n_H=1. Subsensitive responses (i.e., $n_H < 1$) may arise, for example, from the presence of negative cooperativity (2) or negative feedback (3). Systems with transient responses, such as the one we implemented in our three toy models, also known as pulse-generators, can be subsensitive. Given that one of the effects of the PRESS signaling mode is to make the overall response subsensitive (expand the input dynamic range), we asked if the transient responses we implemented are intrinsically subsensitive (i.e., when studied uncoupled from a binding mechanism); and if so, how this subsensitivity contributes to the overall system behavior, when coupled to a slow or a fast binding reaction. With this in mind, in what follows we analyze in detail the model with an inactive refractory state and the model controlled by a negative feedback loop (Models 1 and 3).

Sensitivity in Model 1: X with an inactive refractory state.

In order to study the pulse generator of Model 1 in isolation, that is, independently of the ligand-receptor complex (C) formation, we first studied the peak response of X* as a function of a step increase in C (Fig. S11a). For the parameter values we selected, the system was subsensitive, with a Hill coefficient of 0.8, corresponding to a dynamic range (EC_{90}/EC_{10}) of 243 (colored lines in Fig. S11a), three times the dynamic range of a Michaelian response (81, black line). We tested three values of r_2 (the rate of inactivation of X*, the key parameter controlling the duration of the pulse response), which had no significant impact on the n_H, but had a strong effect on the EC_{50} of the response.

Next, we introduced a simple ligand-receptor binding reaction between the step input and the X cycle, using fast or slow ligand-receptor binding rates (Fig. S11b and c). The addition of the ligand-receptor binding reaction increased the sensitivity from 0.8 to 0.9 when we used fast ligand binding rates (reducing the dynamic range to ~132), and decreased it to 0.7 when we used slow binding rates (increasing the dynamic range to ~533) (Table S1). In both cases, parameter r_2 had no significant impact on the n_H, impacting strongly on the EC_{50} of the response.

These results indicate that the coupling of a ligand-receptor reaction interacts with the subsensitive pulse-generator, in a manner that depends on the speed of this reaction. When binding is fast, the

overall sensitivity is increased, but when binding is slow, it is further decreased. The speed of the binding reaction also affects the degree of the dynamic range displacement; it was much greater with slow binding than fast binding. Thus, we conclude that the intrinsic subsensitivity of the pulse generator does not explain the effects observed in PRESS mode of signaling.

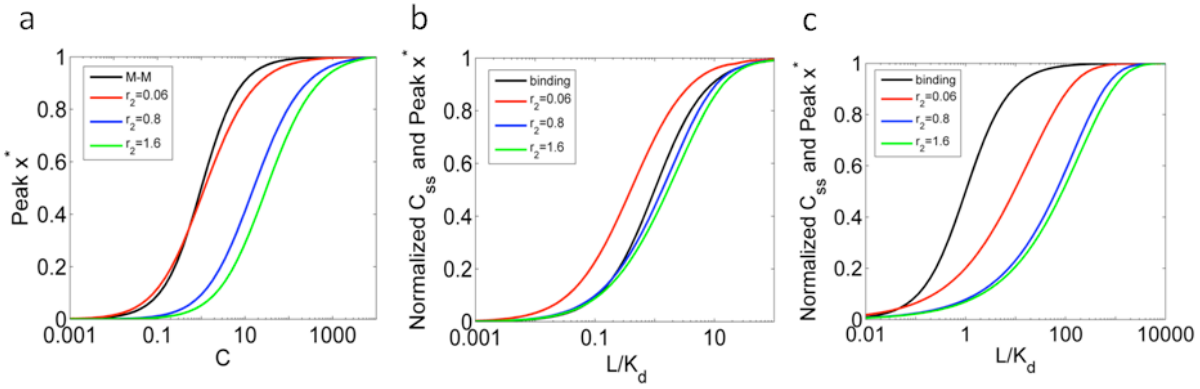

Figure S11. Sensitivity in Model 1

X with an inactive refractory state. Parameters: X_{tot}=10, r_1=0.1, r_2=0.06-0.8-1.6 (red, blue, green lines), r_3=0.001. a. The isolated cycle of X (no dynamics of ligand-receptor complex, C, formation). Plot shows peak response of X* as a function of step increase in C. A Michaelian response (with EC_{50}=1 and n_H=1) is included with a black line. b-c. Complete Model 1 (including the dynamics of ligand-receptor complex, C, formation). Plots show peak response of X* as a function of the ligand concentration, L (L normalized by the K_d of the ligand-receptor reaction). Different values of parameter r_2 are included in different colors, as indicated. Rates in b are k_+=0.02 $(nM*sec)^{-1}$, k_- =0.1 sec^{-1} and in c k_+=0.0002 $(nM*sec)^{-1}$, k_-=0.001 sec^{-1}.

	C as the stimulus		Fast binding		Slow binding	
r_2	EC_{50}	n_H	EC_{50}	n_H	EC_{50}	n_H
0.06	1.2	0.79	0.4	0.92	9.3	0.71
0.8	15.9	0.80	1.3	0.94	65.1	0.75
1.6	31.3	0.81	1.7	0.92	87.2	0.73

Table S1. Model 1 sensitivity.

Characterization of the potency (EC_{50}) and sensitivity (n_H) for the different curves in Fig. S11, as a function of parameter r_2, corresponding to Model 1.

Sensitivity in Model 3: X controlled by a negative feed-back loop (NFBL).

We performed the same study for Model 3. When considered in isolation, for the parameter values we selected, the peak response of X* to a step increase in C (Fig. S12) resulted ultrasensitive, with an n_H of 1.7, corresponding to a dynamic range of 13.3, and an EC_{50} of 0.3. When we included the dynamics of ligand-receptor formation (C), the sensitivity of the overall system decreased to 1.3 for fast binding, and even further to 1.2 for slow binding (Table S2), corresponding to a dynamic range of 29.4 and 38.9, respectively. In addition, the dynamic range of C (EC_{50}) was displaced from 1 to 4.5 for fast binding and from 1 to 447.6 with slow binding.

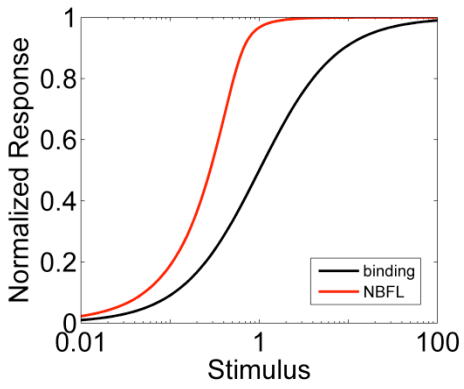

Figure S12. Sensitivity in Model 3

X controlled by a negative feed-back loop (NFBL). Parameter values: k_{XB}=1, K_{XB}=0.01, k_{FBB}=5, K_{FBB}=100, F_B=0.5, k_{CX}=5, K_{CX}=0.1, k_{BX}=6, K_{BX}=0.01. A Michaelian response (with EC_{50}=1 and n_H=1) is included with a black line. The response of the NFBL to a step increase in C (indicated as Stimulus)

C as the stimulus		Fast binding		Slow binding	
EC_{50}	n_H	EC_{50}	n_H	EC_{50}	n_H
0.3	1.71	4.5	1.31	447.6	1.24

Table S2. Model 3 sensitivity.

Characterization of the displacement (EC_{50}) and dynamic range (n_H) for the different curves in Fig. S1B and in Fig. S12, corresponding to Model 3.

General conclusions based on the above studies and the results in the main text:

i) The **ligand-receptor binding** reaction has an equilibrium dose-response curve characterized by n_H = 1 and EC_{50} = 1 (dose = ligand/K_d, response = normalized ligand-receptor complex). The dose-response curve before reaching equilibrium has n_H > 1 and EC_{50} > 1 (see SI Appendix, Section 1), that is, it is displaced to the right and has smaller input dynamic range (increased sensitivity). Therefore, the shape of the binding dose response curve by itself cannot explain the overall characteristics of PRESS systems.
ii) **Pulse generators** may by subsensitive (n_H < 1), such as in Model 1 or ultrasensitive (n_H > 1), such as in Model 3, depending on architecture and parameter values.
iii) The **coupled system** (ligand-receptor -> pulse generator) results in a dose-response curve (dose = ligand/K_d, response = maximum value reached by the pulse) whose characteristics depend on the coupling, and particularly on the dynamics of the ligand-receptor reaction.

If the ligand-receptor reaction is fast (compared to the time-scales of the pulse generator), then we may consider the equilibrium ligand-receptor dose-response curve (with $n_{H,A\ fast}$ = 1) as the input to the pulse generator. Therefore, the upper bound of the overall system sensitivity depends exclusively on the sensitivity of the pulse generator. If the ligand-receptor reaction is slow, one may be tempted to think

that the n_H of the dose-reponse that acts as the input to the pulse generator has an $n_{H,A\ slow} > 1$ (according to point i)), resulting in a coupled sensitivity that might be higher for the slow ligand-receptor reaction than for the fast one. This is clearly in disagreement with the results in Tables S1 and S2, where we show that the coupled sensitivity is consistently lower than that of the pulse generator.

What happens is that for each ligand concentration that stimulates the coupled system, the pulse generator reaches its maximum at a different time t_{max} (see right panels in Fig. S1 and also Fig. S13b-d). Particularly, for Model 1, if the input stimulus is large, the peak of X* occurs early; if the input stimulus is small, the peak of X* occurs late. The binding dose-response curve for early times is shifted to the right compared to those of later times, resulting in an effective ligand-receptor curve, that of $C(t_{max})$, that has lower slope than that of C in early times or even than that of C in equilibrium (see Fig. S13a, green line).

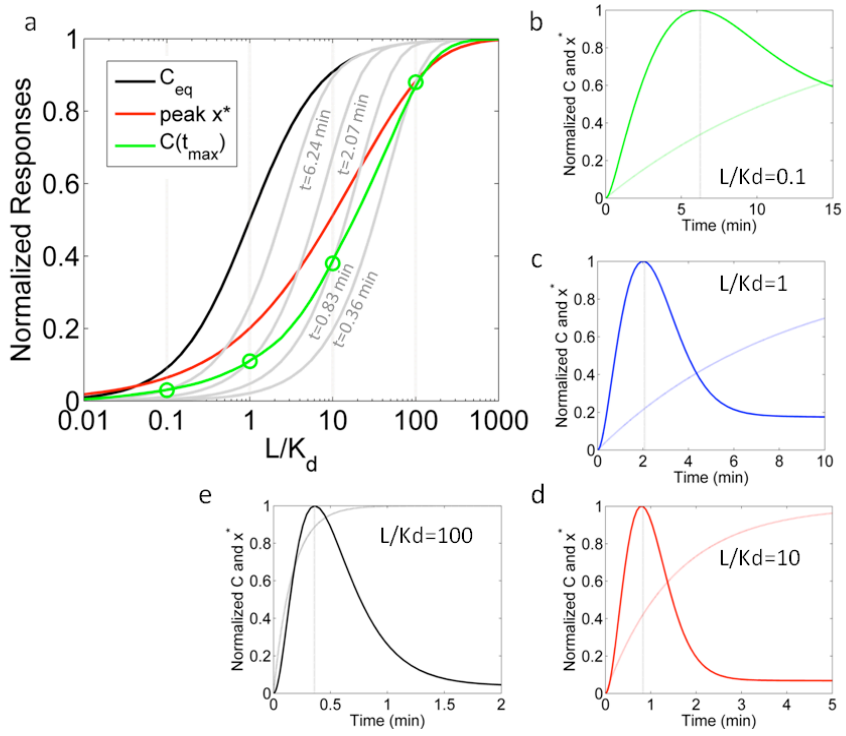

Figure S13. Graphical explanation of the expansion of the input dynamic range. Analysis of the sensitivity of the ligand-receptor system coupled to the pulse generator in Model 1. Parameters: X_{tot}=10, r_1=0.1, r_2=0.06, r_3=0.001, k.=0.001 sec^{-1}. **a**. Normalized ligand-receptor complex C in equilibrium (black), at four different times indicated over the figure (grey), and for the times where the maximum of the pulse occurs for each dose, C(tmax) (green). Peak X* is included in red. The horizontal axis corresponds to the dose of ligand normalized by the K_d of the ligand-receptor reaction. The times selected to plot C versus L/K_d before equilibrium are the t_{max} for L/K_d=0.1, 1, 10, 100: 6.24, 2.07, 0.83, and 0.36 min respectively. Green circles indicate the intersection of doses L/K_d=0.1, 1, 10, 100, and C vs L/K_d at the listed times, therefore, those circles are over the curve C(tmax). The curve C(tmax) vs L/K_d is characterized by E_{C50}=17.7 and n_H=0.9. **b-e**. Temporal profiles for normalized C (thin line) and peak X* (thick line) for doses L/K_d=0.1, 1, 10, 100.

The coupled sensitivity for the ligand-receptor -> pulse generator system is then bounded by the n_H of the curve formed by the $C(t_{max})$ values (Fig. S13). So, **for a pulse generator and a slow ligand-receptor reaction, the coupled sensitivity will be lower than that of the pulse generator in isolation, whether or not the sensitivity of this last one is lower or greater than 1**. Therefore, PRESS itself lowers the sensitivity of the overall response, expanding its dynamic range.

In the case of Model 3, **the pulse generator reaches its maximum at similar times t_{max}**: 0.88, 1.1, 1.3 sec for normalized doses: 1500, 500, 100, as indicated in Fig. S14, resulting in an effective ligand-receptor curve, that of $C(t_{max})$, that has not a much lower slope than that of each C(t) curve (curves in grey). The overall result for

this model is then, that the coupled sensitivity is still lower than the sensitivity of the pulse generator considered in isolation but the effect is not as important as when the values of t_{max} are very different for different doses (Model 1, Fig. S13).

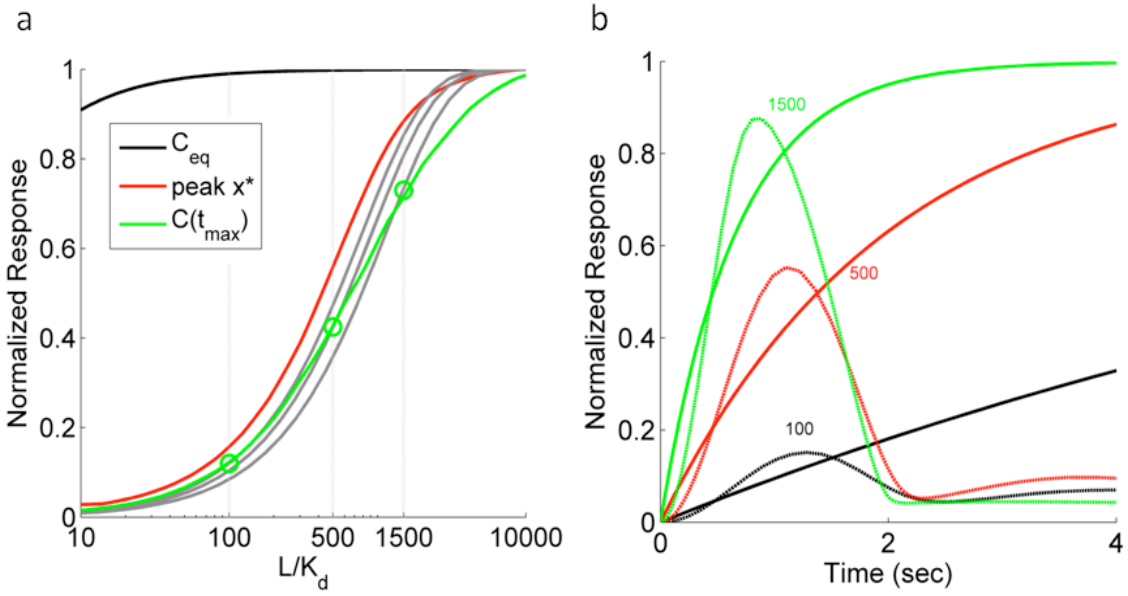

Figure S14. Graphical explanation of the behavior of Model 3.

Analysis of the sensitivity of the ligand-receptor system coupled to the pulse generator in Model 3. Parameters: k_{-}=0.001 sec^{-1}, k_{XB}=1, K_{XB}=0.01, k_{FBB}=5, K_{FBB}=100, F_B=0.5, k_{CX}=5, K_{CX}=0.1, k_{BX}=6, K_{BX}=0.01. **a**. Normalized ligand-receptor complex C in equilibrium (black), at three different times from right to left 0.88, 1.1, 1.3 sec (grey), and for the times where the maximum of the pulse occurs for each dose, $C(t_{max})$ (green). Peak X* is included in red. The horizontal axis corresponds to the dose of ligand normalized by the K_d of the ligand-receptor reaction. The times selected to plot C versus L/K_d before equilibrium are the t_{max} for L/K_d=1500, 500, and 100, respectively. Green circles indicate the intersection of doses L/K_d=100, 500, 1500, and C vs L/K_d at the listed times, therefore, those circles are over the curve $C(t_{max})$. The curve $C(t_{max})$ vs L/K_d is characterized by EC_{50}=666.4 and n_H=1.15. **b**. Temporal profiles for normalized C and peak X* for doses L/K_d=100, 500, 1500.

4. The effect of noise during PRESS

To determine the effect of noise during PRESS, we run stochastic simulations of the toy model labeled as Model 1 in this SI Appendix, Section2 (the model with an inactive refractory state in Fig. 2 of the main text) varying the number of receptors. It is well known that at low concentrations deterministic simulations based on the law of mass action are, in general, unlikely to be applicable. Therefore we used a stochastic approach to describe the binding kinetics and to account for the noise resulting from the probabilistic character of the (bio)chemical reactions. The goal of the study was to introduce different degrees of noise at the ligand-receptor binding step and then analyze whether this noise was amplified or not by the downstream response. To do that, we run simulations with different number of receptors (low, medium or high) while maintaining constant the number of the rest of species in the system.

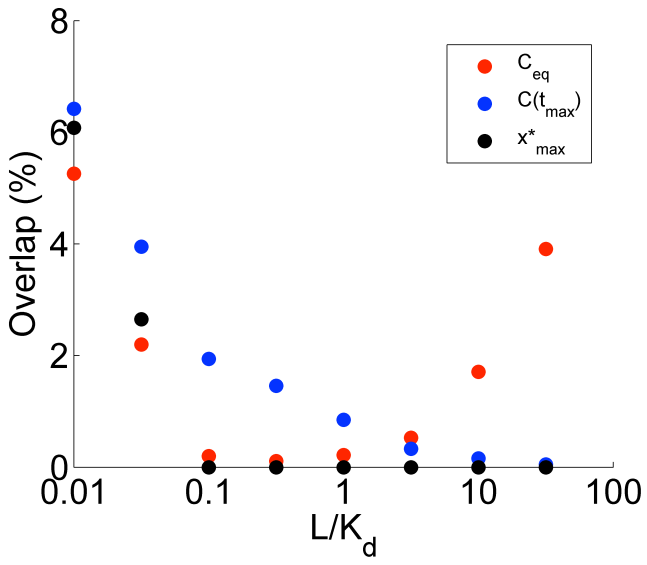

Figure S15. Percentage of overlap between the stochastic outputs of two consecutive doses for R_{tot}=30.

Results of calculating the overlap in the outputs of the 1001 stochastic simulations performed for Model 1 (the model with an inactive refractory state) for low number of receptors (30 receptors per cell), using stochastic methods. Simulations were done in Copasi using its adaptive tau-leaping algorithm. Parameter values: k_+=0.0002 ml/(pmol*sec), k_-=0.001 1/s, r_1=0.01 ml/(pmol*sec), r_2=0.06 1/sec, r_3=0.001 1/sec (with 1 pmol/ml = 1 nM). Initial particle numbers: receptor=30, x=14536.5. Cell volume= 5e-11 ml. The overlap was calculated with three different variables: the equilibrium value of the ligand-receptor complex C (C_{eq}) in red, maximum of X* (X^*_{max}) in black, and C at the time where X* reaches its maximum ($C(t_{max})$) in blue. Labels in horizontal axis indicate the lower dose of the two doses being compared for the overlap, normalized by the K_d of the ligand-receptor reaction. Doses being compared are (in units of K_d): 0.01, 0.03, 0.1, 0.32, 1.0, 3.16, 10, 31.62, 100.

We include the results of simulating Model 1 for low, medium, and high number of receptors (30-300-3000), using stochastic methods, in Fig. S2. We performed numerical simulations in Copasi 4.11 (4) using its adaptive tau-leaping algorithm. Importantly, we defined parameter r_1 (x* activation rate) as 0.1/initial free receptor, and therefore its value was 0.1/30, 0.1/300, and 0.1/3000, respectively. Thus, each bound receptor has a stronger activation capacity when there are only 30 total receptors than when there are 300 or 3000. In this way, the effective activation rate of X* is comparable between the simulations with different number of receptors.

As expected, the effect of noise is much more evident when the number of receptors is low, see Fig. S2, as can be seen both in the temporal profiles on the right panels, and in the standard deviation from 1001 simulations plotted

on the left panels. The square of the coefficient of variation plotted in the bottom panel indicates that for the three variables, C_{ss} (red curves), $C(t_{max})$ (blue curves), and peak X* (black curves), lower receptor number results in higher CV^2 for the whole range of doses considered. Also, for the three amounts of receptors considered (30 in solid lines, 300 in dashed lines, and 3000 in dotted lines), the curve of C_{ss} is lower than that of peak X*, and peak X* is lower than the curve for $C(t_{max})$. This result suggests that even in the case of very low number of receptors (30 per cell), which introduce a significant noise at the level of occupied receptor (Fig. S2F), the pulse generator downstream of the receptor did not amplify it and therefore the improvement gained by PRESS is not lost or masked by the effects of noise.

In Fig. S15, we show the percentage of overlap between the outputs of 1001 stochastic simulations for two consecutive doses, L_i/K_d and L_{i+1}/K_d, being $L_{i+1}/K_d \sim 3 * L_i/K_d$, evaluated for C_{eq} (red), $C(t_{max})$ (blue) and X^*_{max} (black), in the case of low number of receptors (30 receptors per cell). The aim of this figure is to evaluate if two doses can be identified as different doses based on the information given by each variable, C_{eq}, $C(t_{max})$, X^*_{max}, particularly in the region of high doses ($L/K_d > 1$). The results in Fig. S15 indicate even in this case with significant noise at the level of occupied receptor, variable X^*_{max} has lower overlap than C_{eq}, supporting that the improvement gained by PRESS is not lost by the effects of noise.

5. Mathematical model to study the sensing of a stationary spatial gradient

In what follows we present two alternative mathematical descriptions for the variable Delta. In Description 1 we derived the steady-state concentration of αF as an approximate solution to the diffusion equation from a point source, with, and also without, reflecting boundary conditions on the sensing sphere. Combining this solution with the normalized bound receptor function we derived the variable *Delta* (difference of bound receptors at the front and at the back). In Description 1, *Delta* depends on three combinations of parameters related the average concentration sensed by the cell, the ratio between the radius of the cell and the distant to the source, and the ligand-receptor unbinding rate. In Description 2, we derived variable *Delta* in terms of the maximal and minimal ligand concentrations sensed by the cell, without relating them by any particular function (i.e. without specifying the profile of the gradient). In this case, *Delta* still depends on the ligand-receptor unbinding rate, and on the maximal and minimal ligand concentrations. Description 1 is based on a given source-sensing cell pair, while Description 2 is based on the local environment sensed by the cell. Both descriptions are easily related to one another.

5.1 An analytical expression for the αF gradient generated by a point source, and for the variable Delta (Description 1)

As in Segall (5), the cell is modeled as an impermeable sphere of radius a, with d the distance from the center of the sphere to the point source of αF. There is azimuthal symmetry with respect to the line between the center of the sphere and the point source. The concentration at any point on the sphere will vary with the angle, θ, between the line connecting the center of the sphere to the point source and the line connecting the center of the sphere to the point on the surface. The point over the sphere that is nearest the source is indicated with an **f** (front, θ = 0) and the point that has the greatest distance to the source is indicated with a **b** (back, θ = π).

An approximate solution to the diffusion equation with a point source and given reflecting boundary conditions on the sphere (5) is:

$$\alpha F(\theta) = \frac{q}{4\pi D d}\left[\sum_{j=0}^{\infty}(2j+1)\left(\frac{a}{d}\right)^{j}\frac{P_j(\cos\theta)}{j+1}\right] \quad (3)$$

where αF(θ) is the steady-state concentration of αF as a function of the position over the cell surface, q is the rate of release of alpha-factor from the point source, D is the αF diffusion coefficient, and P_j is the Legendre polynomial of order j (5).

We model the ligand-receptor binding with the following reaction:

$$\alpha F + R \leftrightarrow C \quad (4)$$

where αF is the ligand (alpha-factor), R is the membrane receptor assumed to have a uniform density over the cell surface, C is the complex ligand-receptor, and k_+ and k_- are the binding and unbinding rates, respectively. The dissociation constant K_d is defined as k_-/k_+ and represents the ligand concentration that produces a bound receptor level that is one-half of its maximum. The total concentrations of receptor and ligand in the system are assumed to be constant, $R_{tot} = [R] + [C]$, $\alpha F_{tot} = [\alpha F] + [C]$. Thus, only one concentration of the three ([R], [αF], and [C]) is independent; the other two may be determined from

R_{tot}, αF_{tot} and the independent concentration. The kinetics of this system can be solved analytically. Choosing [C] as the independent concentration and representing the concentrations without the brackets for brevity (e.g. R = [R]), the kinetic rate equation can be written as:

$$\frac{dC}{dt} = k_+ \alpha F\, R - k_- C \cong k_+ \alpha F_{tot}(R_{tot} - C) - k_- C = k_+ \alpha F(R_{tot} - C) - k_- C \qquad (5)$$

where we have assumed that $[\alpha F] \sim \alpha F_{tot}$, meaning that the consumption of ligand in the ligand-receptor reaction is negligible compared with αF_{tot}. αF_{tot} is then the function $\alpha F(\theta)$ given by Eq. (3). The solution for Eq. (5) is:

$$C(\theta, t) = C_{eq}\left(1 - \exp\left(-\frac{t}{\tau}\right)\right), \quad (6)$$

with

$$C_{eq} = R_{tot}\frac{\alpha F(\theta)/K_d}{\frac{\alpha F(\theta)}{K_d}+1} \qquad (7)$$

being the steady-state value for C and

$$\tau = [k_-(1 + \alpha F(\theta)/K_d)]^{-1} \quad (8)$$

the time required for the bound receptor C to rise from zero to 1−1/e (that is, 63.2%) of its final steady-state value.

Combining Eqs. (3), (6), (7), and (8) we obtain that the normalized bound receptor, C/R_{tot} as a function of θ and t depends on the following combination of parameters:

$$p_1 = \frac{\frac{q}{4\pi D d}}{K_d}; p_2 = \frac{a}{d}; p_3 = k_-. \quad (9)$$

Parameter p_1 combines parameters related to the ligand source (q;D), the distance to the source (d), and K_d, and indicates the average concentration sensed by the cell in multiples of K_d, for instance, p_1=1 means that the cell feels a concentration of about 1 × K_d. Parameter p_2 is a geometrical parameter defined as the ratio between the radius of the spherical cell and the distance from the center of the cell to the point source. p_1 and p_2 are dimensionless parameters. Parameter p_3 is the ligand-receptor unbinding rate and has units of 1/time. The three parameters are always positive, and p_2 is such that $0 < p_2 < 1$.

For p_1 = 10 and p_2 = 0.3 (the values used in most of the paper), the total numbers of bound receptors in steady state, for the hemispheres facing and away from the point source, were calculated following (5) by integration over the angles 0 to π/2 radians (0 to 90 degrees) and π/2 to π radians (90 to 180 degrees), respectively. The total number of receptors was assumed to be 8000 (5). The hemisphere nearest the source has 3720 occupied receptors and the hemisphere away from the source has 3531 occupied receptors. The difference between the two sides, 189 receptors, is 2.6% of the total number of occupied receptors.

The variable Delta is defined as Delta(t) = C(θ = 0, t) − C(θ=π, t) (difference of bound receptors at the front and at the back). The effectiveness of PRESS in the context of gradient sensing depends on how much (amplitude) and for how long (duration) lasts the overshoot of Delta(t). Delta depends on parameters p_1, p_2, and p_3.

By combining Eqs. (3), (6), (7), and (8) we numerically compute Delta and determine that the overshoot amplitude increases with the concentration of ligand (which increases p_1). This is because $Delta_{eq}$ has a biphasic behavior with p_1 while $Delta_{max}$ has not (Fig. S16a inset). $Delta_{eq}$ peaks at about p_1=1, i.e. at an average concentration of αF of about the K_d. On the other hand, $Delta_{max}$ is virtually indistinguishable

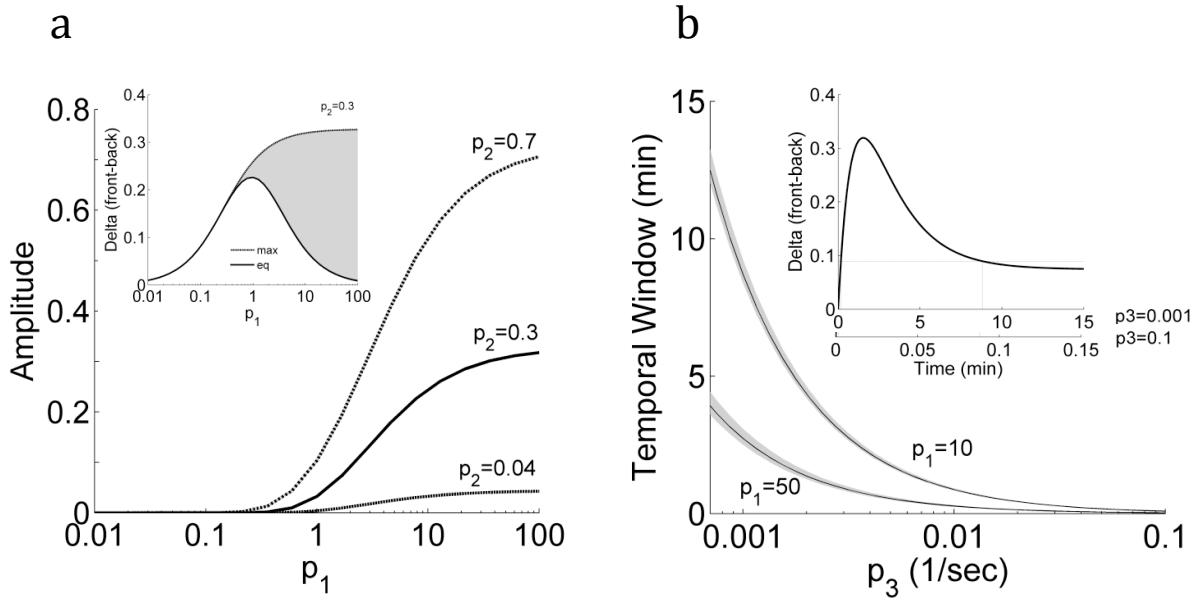

Figure S16. Characterization of PRESS applied to gradient detection.

a. Amplitude of Delta's overshoot as a function of p_1 (average ligand concentration relative to the K_d) for the indicated values of p_2. Overshoot occurs at p_1 greater than ~ 1, providing an advantage of PRESS over equilibrium signaling. p_3 does not affect $Delta_{eq}$ or $Delta_{max}$. **Inset**. Dependency of $Delta_{eq}$ (solid line) and $Delta_{max}$ (dashed line) on parameter p_1 (average concentration of αF) for p_2=0.3. $Delta_{eq}$ is biphasic with p_1 while $Delta_{max}$ is monotonic. The shaded area represents Delta's overshoot. **b**. Temporal window during which Delta overshoots $Delta_{eq}$ as a function of parameter p_3 (the time scale of the αF binding reaction), for p_2=0.3 and the indicated values of p_1. The width of each line (shaded) marks the region between two extremes yeast cell sizes (cells from 1.6 to 6.4 μm diameter, located at a distance from the source of 6.7 μm), corresponding to p_2 from 0.12 to 0.48. **Inset** shows Delta versus time for the two values of p_3 indicated in the x-axis (p_1 = 10, p_2 = 0.3). Graph shows that the temporal profile is independent of p_3, except for the scale of time. We defined the temporal window for PRESS as the interval during which Delta is higher in more than 20% of $Delta_{eq}$.

from $Delta_{eq}$ for low values of p_1, but at p_1 approaching 1 $Delta_{max}$ diverges from $Delta_{eq}$ increasing asymptotically to a maximum $Delta_{max}$. Consequently, at values above 1, increasing p_1 increases the amplitude of the overshoot. In contrast, its duration decreases with p_1 (Fig. S16b). Thus, even though high levels of signal provide greater overshoot amplitude for PRESS, the time window available for PRESS is reduced.

Increasing p_2 for a given value of p_1 (which translates into increasing the sensing cell size), increases both $Delta_{max}$ and $Delta_{eq}$, effectively improving the chances of the cell of detecting differences between front

and back bound receptor, both at equilibrium and prior to it, but it does not make PRESS better than equilibrium signaling (Fig. S16a).

Most interestingly, the duration of Delta's overshoot is most strongly affected by p_3 (Fig. S16b). For Cell 1 in our example of Fig 3B in the main text, a value of p_3 100 times faster than the actual αF binding reaction reduces the time window for PRESS from about 6 minutes to about 0.06 minutes (3.6 seconds) (inset in Fig. S16b). Thus, the slower p_3, the more time there is for PRESS. On the other hand, p_3 does not affect the amplitude of the overshoot.

5.1.1 A simplified formula for the αF gradient generated by a point source, and the variable Delta

If the effect of the reflecting boundary conditions on the sensing sphere is not considered, then the steady-state solution for the problem of diffusion from a point source is simplified to:

$$\alpha F(\theta) = \frac{1}{4\pi D d}\frac{1}{\sqrt{1+(a/d)^2-2(a/d)\cos\theta}}, \quad (10)$$

In terms of parameters p_1, p_2 and p_3, and for the case with reflecting boundary conditions, we have:

$$\frac{\alpha F(\theta)}{K_d} = p_1\left[\sum_{j=0}^{\infty}(2j+1)(p_2)^j\frac{P_j(\cos\theta)}{j+1}\right], \quad (11)$$

and for the case without:

$$\frac{\alpha F(\theta)}{K_d} = p_1\frac{1}{\sqrt{1+(p_2)^j-2p_2\cos\theta}} \quad (12)$$

This last case results in $\alpha F_f = \alpha F(\theta = 0) = p_1/(1 - p_2)$ and $\alpha F_b = \alpha F(\theta = \pi) = p_1/(1 + p_2)$. In Fig. S17 we compare the α-factor profiles over the sensing cell surface with and without reflecting boundary conditions, i.e. we compare Eqs. (11) and (12). If the presence of the sphere is taken into account in the diffusion problem (Eq. (11)), the differences between front and back are greater than if not.

With αF given by Eq. (12) we obtain:

$$\frac{C_f}{R_{tot}} = \frac{p1}{p1+(1-p2)}(1-\exp(-t/\tau_f)) \quad (13)$$

$$\frac{C_b}{R_{tot}} = \frac{p1}{p1+(1+p2)}(1-\exp(-t/\tau_b)) \quad (14)$$

where

$$\tau_f = \frac{1-p2}{p3(p1+1-p2)} \quad (15)$$

$$\tau_b = \frac{1+p2}{p3(p1+1+p2)} \quad (16)$$

resulting in

$$Delta(t) = Delta_{eq} + f(t) \quad (17)$$

$$Delta_{eq} = \frac{2p1p2}{(1+p1)^2-p2^2} \quad (18)$$

$$f(t) = \frac{p1}{1+p1+p2}\exp\left(-tp_3\frac{1+p1+p2}{1+p2}\right) - \frac{p1}{1+p1-p2}\exp\left(-tp_3\frac{1+p1-p2}{1-p2}\right) \quad (19)$$

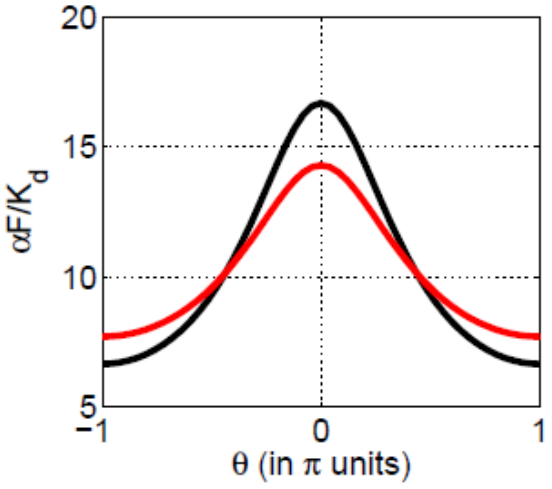

Figure S17. α-factor profiles over the sensing cell surface.
Including (black) not (red) reflecting boundary conditions. αF is normalized by K_d and θ is plotted in π units.

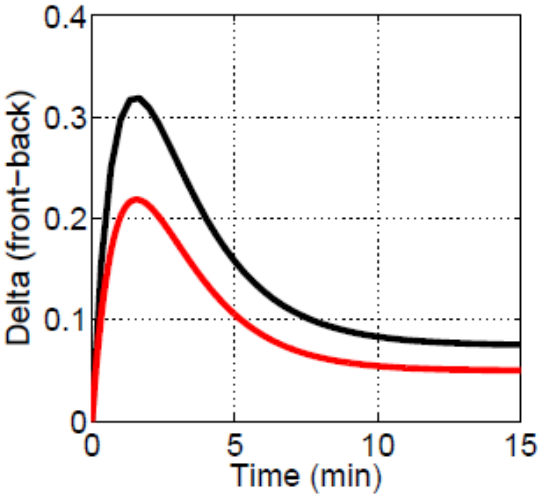

Figure S18. Delta vs. time
Data was calculated with (black) and without (red) reflecting boundary conditions, for p_1=10, p_2=0.3, and p_3=0.001 1/sec.

In Fig. S18 we compare the variable Delta calculated using Eq. (11) or Eq. (12), we can see that in both cases there is a time window where Delta is greater than its steady-state value, meaning that the feature of the overshoot in Delta does not depend on the use or not of reflecting boundary conditions over the sensing sphere.

We make use of this simplified scheme to analytically explain some of the features in Fig. S17. From Eq. (18) we see that $Delta_{eq}$ depends on parameters p_1 and p_2 but not on p_3. Computing the derivative of $Delta_{eq}$ with respect to p_1 and equaling to zero, we obtain that $Delta_{eq}$ reaches a maximum at $p_1\tilde{} = (1 - p_2^2)^{1/2}$, it increases with p_1 for $p_1 < p_1\tilde{}$, then decreases. For a small value of parameter p_2, $p_1\tilde{}$ is close to 1, for instance, for p_2 = 0.3 (the value p_2 used in the majority of the paper), $p_1\tilde{}$ = 0.95. The derivative of $Delta_{eq}$ with respect to p_2 is always positive, meaning that $Delta_{eq}$ always increases with p_2.

Using Eqs. (17)-(19) we can explicitly compute the time t_+ where Delta becomes greater than $Delta_{eq}$, i.e. when f(t) becomes positive:

$$t_+ = \frac{1-p2^2}{2p1p2p3}\log\left(\frac{1+p1+p2}{1+p1-p2}\right) \quad (20)$$

and the time t_{max} where Delta reaches a maximum:

$$t_{max} = \frac{1-p2^2}{2p1p2p3}\log\left(\frac{1+p2}{1-p2}\right) \quad (21)$$

The maximum value reached by Delta is given by $Delta_{max}$ = Delta(t = t_{max}):

$$Delta_{max} = Delta_{eq}\left(1 + \frac{p1}{1+p2}\exp\left[\frac{-(1-p2)(1+p1+p2)}{2p1p2}\log\left(\frac{1+p2}{1-p2}\right)\right]\right). \quad (22)$$

$Delta_{max}$ depends on parameters p_1 and p_2 but not on p_3. By plotting $Delta_{max}$ versus parameter p_1 for different values of p_2, or $Delta_{max}$ versus parameter p_2 for different values of p_1 (not shown), we can see that it increases monotonically with both p_1 and p_2. From this last equation we see that for small values of p_1, the second term inside the parenthesis is very small resulting in $Delta_{max} \sim Delta_{eq}$.

5.2 An analytical expression for the variable Delta (Description 2)

The effectiveness of PRESS in the context of gradient sensing depends on the **amplitude** and **duration** of the overshoot of Delta(t). Thus, we developed a mathematical analysis to describe the evolution over time of Delta(t), assuming homogeneously distributed receptors and simple binding kinetics. Delta(t) depends on the properties of the gradient: the maximum and minimum ligand concentrations sensed by the cell (in the case of αF, $\boldsymbol{\alpha F_f}$ and $\boldsymbol{\alpha F_b}$, the front and back αF concentrations, respectively), as well as of the sensing cell: the binding and unbinding rate for the ligand-receptor reaction, $\mathbf{k_+}$ and $\mathbf{k_-}$. Normalizing by R_{tot} we obtain Delta(t) as follows:

$$\mathrm{Delta}(t) = \frac{\widetilde{\alpha F}_f - \widetilde{\alpha F}_b}{(1+\widetilde{\alpha F}_f)(1+\widetilde{\alpha F}_b)} + \frac{\widetilde{\alpha F}_b}{1+\widetilde{\alpha F}_b}\exp\{-t[k_-(1+\widetilde{\alpha F}_b)]\} - \frac{\widetilde{\alpha F}_f}{1+\widetilde{\alpha F}_f}\exp\{-t[k_-(1+\widetilde{\alpha F}_f)]\}$$

Where $\widetilde{\alpha F}_f$ and $\widetilde{\alpha F}_b$ are the front and back concentrations of αF normalized by the dissociation constant, K_d. The first term (in black) does not depend on time, and it corresponds to the value of Delta(t) at equilibrium, $Delta_{eq}$. The second and third terms (in blue and red) correspond to the dynamics of binding at the back (in blue) and the front (in red). We then derived a formula for $Delta_{max}$, the maximum value of Delta(t), its difference with $Delta_{eq}$ define the overshoot; and t_{max}, the time of $Delta_{max}$, with which we obtained the overshoot's duration (arbitrarily defined as temporal window during which Delta(t) is 20% larger than $Delta_{eq}$).

The function Delta(t) can be characterized by:

1) its initial value, Delta(t=0)=0;

2) its asymptotic value, Delta(t->∞):

$$\mathrm{Delta}_{eq} = \frac{\widetilde{\alpha F}_f - \widetilde{\alpha F}_b}{(1+\widetilde{\alpha F}_f)(1+\widetilde{\alpha F}_b)};$$

3) the time t_{max} where Delta(t) reaches a maximum:

$$t_{max} = \frac{1}{k_-(\widetilde{\alpha F}_f - \widetilde{\alpha F}_b)}\log\left(\frac{\widetilde{\alpha F}_f}{\widetilde{\alpha F}_b}\right);$$

4) the maximum value reached by Delta(t) , given by $Delta_{max}$ = Delta(t = t_{max}):

$$\mathrm{Delta}_{max} = \mathrm{Delta}_{eq} + \left\{\frac{\widetilde{\alpha F}_b}{1+\widetilde{\alpha F}_b}\exp\left[-\frac{1+\widetilde{\alpha F}_b}{(\widetilde{\alpha F}_f - \widetilde{\alpha F}_b)}\log\left(\frac{\widetilde{\alpha F}_f}{\widetilde{\alpha F}_b}\right)\right] - \frac{\widetilde{\alpha F}_f}{1+\widetilde{\alpha F}_f}\exp\left[-\frac{1+\widetilde{\alpha F}_f}{(\widetilde{\alpha F}_f - \widetilde{\alpha F}_b)}\log\left(\frac{\widetilde{\alpha F}_f}{\widetilde{\alpha F}_b}\right)\right]\right\}$$

5) the time t_+ where Delta becomes greater than $Delta_{eq}$:

$$t_+ = \frac{1}{k_-\left(\widetilde{\alpha F}_{f-}\ \widetilde{\alpha F}_b\right)} \log\left(\frac{\widetilde{\alpha F}_f}{\widetilde{\alpha F}_b}\frac{1+\widetilde{\alpha F}_b}{1+\widetilde{\alpha F}_f}\right)$$

6) the temporal window where Delta is greater than $Delta_{eq}$, approximated as $\Delta t=2*(t_{max}-t_+)$:

$$\Delta t = \frac{2}{k_-\left(\widetilde{\alpha F}_{f-}\ \widetilde{\alpha F}_b\right)} \log\left(\frac{1+\widetilde{\alpha F}_f}{1+\widetilde{\alpha F}_b}\right)$$

The main quantities in the context of PRESS and the overshoot in Delta(t) are $Delta_{max}$, $Delta_{eq}$ and the temporal window Δt, where Delta(t) is greater than $Delta_{eq}$. $Delta_{max}$ and $Delta_{eq}$ depend on $\widetilde{\alpha F}_f$ and $\widetilde{\alpha F}_b$ only, and Δt depends on those two quantities and also on k_-. Linear and exponential gradients are represented in the $(\widetilde{\alpha F}_b, \widetilde{\alpha F}_f)$ plane as lines parallel to the identity with different y-intercepts, or lines with zero y-intercept and different slopes, respectively, as described with the following equations:

linear gradient: $\widetilde{\alpha F} = a_1 x + b_1$, $\widetilde{\alpha F}_f = \widetilde{\alpha F}_b + a_1(x_f - x_b)$, $\widetilde{\alpha F}_f = \widetilde{\alpha F}_b + const_1$,

exponential gradient: $\widetilde{\alpha F} = a_2 e^{-x/b_2}$, $\widetilde{\alpha F}_f = \widetilde{\alpha F}_b e^{-\frac{(x_f - x_b)}{b_2}}$, $\widetilde{\alpha F}_f = \widetilde{\alpha F}_b * const_2$ (with $const_2>1$)

The biological relevance of the overshoot's duration depends on the time-scale of the processes downstream to the ligand-binding reaction (i.e., is the downstream process fast enough to generate a response during the temporal window where Delta(t) > $Delta_{eq}$?). The values of Delta(t) are differences between the fraction of bound receptor at the front and back, and whether a given value of Delta provides enough directional information to detect a given gradient depends on the particular mechanism of polarization.

To show the behavior of $Delta_{eq}$, $Delta_{max}$, and the overshoot's duration as a function of the gradient, we focused on the case of yeast mating pheromone gradient detection. In **Fig. S3 A-C** we show heatmaps where the color scale indicates $Delta_{eq}$, $Delta_{max}$ and the overshoot's duration, respectively, for a range of gradients (αF front, αF back pair combinations) in a region of αF concentrations from 1 to 20 K_ds. For $Delta_{eq}$ and $Delta_{max}$, given a value of αF at the back, increasing αF at the front improves both $Delta_{eq}$ and $Delta_{max}$ (and the same is true for a given value of αF front but decreasing αF back), indicating that, as expected, a more pronounced gradient improves $Delta_{eq}$ and $Delta_{max}$.

We considered the profile of Delta(t) for a cell located in an exponential gradient at an average ligand concentration of ~1×K_d (see Fig. 3, main text). In this case, a cell reaches a value of $Delta_{eq}$ = 0.23. For heuristic reasons, we used this value as reference point, assuming that a value of Delta of 0.23 or larger provides enough front-back difference to distinguish the direction of the gradient, and that values lower than 0.23 result in suboptimal gradient detection. The region to the left of the contour line in **Fig. S3 A** gives all combinations of αF front-αF back that would lead to consistent gradient detection if only equilibrium information is used. However, the region of αF front-αF back combinations where $Delta_{max}$ is greater than 0.23 is much larger than thatobtained if we consider equilibrium binding information (dashed contour line in **Fig. S3 B** marks combinations with $Delta_{max}$ of 0.23). In the region between the $Delta_{eq}$ and $Delta_{max}$ lines of 0.23, pre-equilibrium information is sufficient ($Delta_{max}$>0.23) but equilibrium information is not ($Delta_{eq}$<0.23). In **Fig. S3 C** we show the temporal window where this amplification of the differences between front and back occurs. For the region between the $Delta_{eq}$ and

$Delta_{max}$ lines, the temporal window is not smaller than 6.8 min. The duration of Delta's overshoot is strongly affected by k_-: a value of k_- 100 times faster than the reported αF binding reaction reduces it by a factor 100 (duration reaches a maximum of 15 min for k_-=0.001 sec^{-1}, but only of 0.15 min for k_-=0.1 sec^{-1}). Thus, the slower k_-, the more time available for PRESS. On the other hand, k_- does not affect the amplitude of the overshoot (see formula for $Delta_{max}$ above).

With this analysis, we studied Delta(t) in different gradient situations. We show that the average concentration establishes a tradeoff between overshoot's amplitude and duration. $Delta_{max}$ is larger at higher average ligand concentrations, but the temporal windows are shorter (see grey lines in **Fig. S3 B and C**). The optimal condition depends on the downstream process time scale and sensitivity.

Summarizing:

- $Delta_{eq}$ and $Delta_{max}$ depend only on $\widetilde{\alpha F}_b$ and $\widetilde{\alpha F}_f$. A higher average αF concentration and a more pronounced gradient are conditions that favor $Delta_{eq}$ and $Delta_{max}$.
- The temporal window for PRESS depends on $\widetilde{\alpha F}_b$ and $\widetilde{\alpha F}_f$ and also on the unbinding rate for the receptor-αF reaction, k_- (at a fixed K_d). It is shorter for higher averages of αF concentration and for faster unbinding rates.

6 Supplemental experimental procedures

6.1 Strains and plasmids.

Strains are detailed in Table S3. YACL379 was used as the parental strain, which is a Δ*bar1* strain derived from YAS245-5C (*can1::HO-CAN1 ho::HO-ADE2 ura3 ade2 leu2 trp1 his3*), which in turn is a W303-1a descendant (6).

ESY3136 was made by transforming YACL379 using a PCR product containing the YFP gene followed by the *S. pombe his5+* gene. We directed recombination downstream of the *STE20* gene using primers with 40 nt of homology with the 3'end of the *STE20* ORF (7). MWY003 was made in two steps. First, *STE5* was deleted using a PCR product containing the nourseothricin (NAT) resistance gene obtained using primers with 40 nt of homology with the 5' and 3' ends of the *STE5* ORF. Then, this strain was transformed with a pRS404 plasmid containing the *STE5* gene (from -1193 to the end of the ORF) followed by three copies of *YFP*, linearized at the *STE5* promoter with PacI. The fluorescence level of MWY003 is three times that of other colonies aislated from this transformartion, suggesting that three integrations of the *STE5*-YFPx3 construct ocurred. YAB3725 was made by transforming YACL379 with plasmid pBB-Ste2(T305)-CFP linearized with ClaI. pBB-Ste2(T305)-CFP is a pRS406 based plasmid that contains a 514 nt fragment of *STE2* (from nt +402 to +916 counting from the START codon) followed by *CFP*. In this plasmid, ClaI cuts within the *STE2* fragment, and therefore, it integrates at the *STE2* locus, generating a strain that expresses only a Ste2 protein truncated at T305 followed by CFP.

Table S3. Strains.

Strain	Relevant Genotype	Reference
YACL379	*MATa Δbar1*	(6)
ESY3136	*MATa Δbar1 ste20::STE20-YFP::his5+*	This study
MWY003	*MATa Δbar1 Δste5::Nat, (trp1::STE5-YFPx3::TRP1)x3*	Peter Pryciak lab
YAB3725	*MATa Δbar1 ste2::P_{STE2} STE2(T305)-CFP::URA3*	This study
YGV5097	*MATa Δbar1 BEM1::BEM1-3xmNeonGreen-HIS3MX6*	This study

We made YGV5097 by PCR-based gene tagging (7) of the *BEM1* ORF in strain ACL379. For the PCR, we used pFA6a-mNG(3x)-KANMX6 as template and two primers with 40nt homology 5'ends to the 3' end of BEM1 ORF and its 3'UTR, respectively. We made pFA6a-mNG(3x)-KANMX6 in two steps. First, we designed and ordered the synthesis of a DNA sequence coding for a tandem repeat of three monomeric NeonGreen (mNG) fluorescent proteins (8) flanked by a 5' PacI and 3' AcsI (Integrated DNA Technologies, Inc., Coralville, Iowa). For this design we optimized codon usage for yeast. For preventing

intra-repeat recombination, we designed each copy of mNG to use slightly different codons. The resulting plasmid is called pUCIDT-mNG(3x). In a second step, we subcloned a PacI and AscI cut fragment containing mNG-(3X) from pUCIDT-mNG(3x) into the pFA6-GFP-HIS3MX6 backbone also digested with PacI and AscI to release the GFP sequence. Finally, the PCR product was used for transformation of ACLY379.

6.2 Quantification of Polarization Times

Microscopy experiments were performed as described elsewhere (9, 10). Exponential growing cells were placed in 384-well glass-bottom plates pre-treated with 1mg/ml of concanavalin A (Sigma) to affix cells. Images were acquired using an Olympus FV1000 confocal module mounted on an Olympus IX-81 microscope, with an Olympus UplanSapo 63x objective (NA = 1.35).

Cells were stimulated with 1µM α-factor at time zero and the same field was followed for up to 2.5 hours. Transmission and YFP (excitation 515nm, emission 530-630nm) images were analyzed by our software Cell-ID (10), identifying individual cells. Using our package Rcell (http://cran.r-project.org/), we created transmission image montages as the ones showed in Fig 3F. Based on these montages, the position in the cell cycle for each cell was manually determined; pre-start cells (G1) responded to pheromone directly while post-start cells (S) budded and finished a round of replication before responding to pheromone (Fig S4A). Analogously image montage for YFP channel (as the one showed in Fig. S4B) were created with Rcell. To avoid missing out-of-focus polarizations, a Z stack was acquired at each time. Polarization time was determined as the first time in which a sustained polarization was observed, for example 16.5 minutes in Fig. S4B. To avoid any bias, the cell-cycle and polarization-time determinations were done independently, and the order in which the cells were presented was randomized.

Three independent repetitions of each strains were done, finding very good repeatability. To estimate the uncertainty in the cumulative polarization curves (Fig. S4C), repetitions were pooled and 95% confidence intervals were calculated from 1000 bootstrap samples (11).

7. Triple monomeric NeonGreen DNA sequence.

ATGGTCTCAAAAGGGGAGGAGGACAACATGGCATCCTTGCCAGCAACTCACGAATTACATATTTTCGGAAGTATTAATGGTGT
TGACTTTGATATGGTTGGACAAGGCACTGGTAATCCAAACGATGGATACGAGGAACTTAATCTTAAATCAACAAAAGGCGATT
TGCAATTTTCCCCCTGGATTCTTGTGCCCCATATTGGGTACGGCTTTCATCAATATTTACCTTACCCTGATGGAATGAGTCCATTT
CAAGCCGCTATGGTAGACGGTTCTGGCTACCAAGTTCATAGAACCATGCAGTTTGAAGACGGCGCTTCCTTAACAGTAAACTA
CAGGTACACGTACGAGGGTTCCCATATTAAGGGAGAAGCCCAAGTTAAGGGTACTGGTTTTCCGGCTGATGGTCCCGTTATGA
CTAATAGCCTGACAGCTGCTGACTGGTGTAGGTCTAAAAAGACATATCCTAACGATAAAACAATAATTTCAACTTTTAAGTGGT
CTTATACCACTGGCAATGGTAAAAGATACAGATCCACTGCCCGTACTACGTATACATTCGCTAAACCAATGGCCGCTAATTATC
TTAAAAATCAACCCATGTACGTGTTTAGGAAGACTGAACTAAAACATAGTAAGACCGAGTTGAACTTTAAGGAATGGCAAAAA
GCCTTCACCGATGTCATGGGAATGGATGAATTATATAAGATGGTTTCCAAGGGTGAGGAAGATAATATGGCATCTTTGCCAGC
CACACACGAATTGCACATATTTGGTTCTATTAATGGAGTGGACTTCGATATGGTGGGTCAAGGTACTGGCAACCCTAATGACG
GATATGAAGAACTTAATCTGAAGTCTACCAAAGGCGATTTACAGTTTTCTCCTTGGATCTTAGTTCCTCATATCGGCTATGGTTT
CCATCAATACTTGCCTTACCCGGATGGTATGAGCCCGTTTCAAGCTGCGATGGTAGATGGTTCAGGTTATCAAGTCCATAGAAC
CATGCAATTTGAAGACGGTGCGTCTTTAACTGTAAATTACAGATACACTTATGAAGGTTCACACATTAAAGGAGAAGCTCAAGT
TAAAGGTACAGGCTTTCCAGCAGATGGTCCTGTCATGACCAATTCTCTAACAGCTGCTGATTGGTGTAGATCAAAAAAGACTTA
CCCAAACGATAAAACAATTATATCTACCTTTAAATGGTCCTACACTACTGGCAATGGTAAAAGATACAGGAGCACTGCTCGTAC
TACTTACACGTTCGCTAAACCGATGGCTGCAAATTACTTGAAAAATCAACCAATGTATGTATTTAGAAAAACTGAATTGAAGCA
TTCTAAAACAGAGCTTAACTTTAAAGAATGGCAAAAAGCATTCACAGACGTTATGGGCATGGACGAATTGTATAAAATGGTCT
CTAAGGGTGAAGAAGATAATATGGCGTCTCTACCAGCTACACACGAACTGCATATCTTCGGTAGCATCAACGGTGTAGACTTC
GATATGGTCGGACAAGGCACCGGAAACCCAAATGATGGGTATGAAGAATTGAACCTAAAGTCAACGAAGGGTGACTTACAGT
TTAGCCCTTGGATTCTAGTGCCACACATTGGTTATGGTTTTCATCAATACCTACCTTACCCCGACGGAATGTCACCATTTCAAGC
CGCTATGGTTGATGGTTCCGGTTATCAAGTTCACAGAACTATGCAGTTTGAAGATGGAGCTTCCCTGACTGTCAACTACAGGTA
CACTTACGAAGGTTCTCATATCAAGGGTGAAGCACAAGTTAAAGGAACCGGTTTTCCTGCCGATGGACCCGTTATGACTAACTC
TTTGACGGCTGCCGATTGGTGCAGGAGTAAAAAGACCTACCCAAACGATAAAACTATCATCAGCACTTTTAAGTGGTCATATAC
TACCGGGAACGGAAAGAGATATAGATCAACCGCTAGAACGACATACACATTTGCCAAGCCTATGGCAGCTAACTACTTAAAAA
ATCAACCTATGTACGTGTTTCGTAAAACCGAATTGAAGCATAGCAAGACAGAATTAAATTTCAAGGAATGGCAAAAAGCCTTC
ACCGATGTTATGGGTATGGACGAACTTTATAAATAG

8. Supplemental References

1. Ma W, Trusina A, El-Samad H, Lim W, & Tang C (2009) Defining network topologies that can achieve biochemical adaptation. *Cell* 138(4):760-773.
2. Koshland DE, Jr., Goldbeter A, & Stock JB (1982) Amplification and adaptation in regulatory and sensory systems. *Science* 217(4556):220-225.
3. Ferrell JE (2001) Regulatory Cascades: Function and Properties. *eLS*, (John Wiley & Sons, Ltd).
4. Hoops S*, et al.* (2006) COPASI--a COmplex PAthway SImulator. *Bioinformatics* 22(24):3067-3074.
5. Segall JE (1993) Polarization of yeast cells in spatial gradients of alpha mating factor. *Proc Natl Acad Sci U S A* 90(18):8332-8336.
6. Colman-Lerner A*, et al.* (2005) Regulated cell-to-cell variation in a cell-fate decision system. *Nature* 437(7059):699-706.
7. Longtine MS*, et al.* (1998) Additional modules for versatile and economical PCR-based gene deletion and modification in Saccharomyces cerevisiae. *Yeast* 14(10):953-961.
8. Shaner NC*, et al.* (2013) A bright monomeric green fluorescent protein derived from Branchiostoma lanceolatum. *Nature methods* 10(5):407-409.
9. Bush A, Chernomoretz A, Yu R, Gordon A, & Colman-Lerner A (2012) Using Cell-ID 1.4 with R for microscope-based cytometry. *Current protocols in molecular biology / edited by Frederick M. Ausubel ... [et al* Chapter 14:Unit 14 18.
10. Gordon A*, et al.* (2007) Single-cell quantification of molecules and rates using open-source microscope-based cytometry. *Nat Methods* 4(2):175-181.
11. Efron B & Tibshirani R (1994) *An introduction to the bootstrap* (Chapman & Hall, New York) pp xvi, 436 p.